Physica A 676 (2025) 130882

Contents lists available at ScienceDirect

Physica A: Statistical Mechanics and its Applications

journal homepage: www.elsevier.com/locate/physa

Nucleation kinetics in phase transformations with spatially correlated nuclei

Massimo Tomellini

Dipartimento di Scienze e Tecnologie Chimiche, Università di Roma Tor Vergata, Via della Ricerca Scientifica 1, 00133 Roma, Italy

ARTICLE INFO

Keywords:
Nucleation kinetics
Non-random nucleation
Phase transition kinetics
Hard-sphere interaction
Kolmogorov-Johnson–Mehl–Avrami (KJMA) model

ABSTRACT

Phase transitions by nucleation, growth and impingement between growing nuclei can occur by nonrandom arrangement of the nuclei. In this contribution, a theoretical approach for the kinetics of phase transition with spatially correlated nuclei by progressive nucleation is developed. The approach is based on the assumptions by Kolmogorov, Johnson, Mehl and Avrami (KJMA) for phase transition kinetics, except for the randomness condition on nucleation that is removed. The work focuses on the rate of formation of the actual nuclei, a quantity that is necessary for describing the transformation kinetics. The approach uses correlation functions, and it is applied to treat hard-sphere interaction between nuclei. Computations have been performed for 2D and 3D growths by truncation of the series expansion in correlation functions up to second order terms. It is shown that the nucleation kinetics undergoes a transition from a typical Random Sequential Adsorption (RSA) behavior to one that is like the KJMA kinetics. The time evolution of the volume fraction of the new phase is found to depend slightly on correlation radius. Such behavior is explained by the partial balancing between the reduction in number density of nuclei and the decrease in impingement events, which have opposite effects on the kinetics.

1. Introduction

Phase transformations of the nucleation and growth-type are driven by the formation of the smallest stable aggregates of the product phase (nuclei) that subsequently grow. In classical theory the process of nucleation takes place by thermal fluctuations in the homogeneous metastable parent phase. Because of these fluctuations, critical-sized aggregates of the new phase form that are potentially stable and become supercritical by addition of monomers. These nuclei can grow with a continuous decrease of free energy. The theory is formulated in terms of a few parameters and allows determining the number of nuclei of the new phase appearing per unit of time and volume [1]. Several excellent reviews are available on the kinetics of homogeneous and heterogeneous nucleation stage [1–3], also for transformations at the solid state where, upon growth and crystal collisions, two mechanisms are singled out, namely *coalescence* and *impingement* [4–6]. The former refers to a collision process followed by a redistribution of matter among particles with mass and shape conserved, while in the latter no redistribution of matter occurs at all. Although the nucleation and growth processes require different approaches, both must be considered for describing the whole kinetics of transformation. To this end, a suitable indicator of the degree of advancement of the transformation is the amount of the product phase, a quantity that is experimentally accessible [1,4,7]. In this context, the phenomenological theory developed by Kolmogorov, Johnson, Mehl and Avrami (KJMA) [8–10] is a useful tool in Materials Science for describing the kinetics of transformations by nucleation and growth [11–16]. Although the

E-mail address: tomellini@uniroma2.it.

https://doi.org/10.1016/j.physa.2025.130882
Received 15 May 2025; Received in revised form 24 July 2025;
Available online 8 August 2025

model was originally formulated in the ambit of phase transitions at the solid state, since then it has been successfully applied to a variety of fields, which include, just to cite a few, Biology, Cosmology, Social Science and Economics [17].

In the KJMA model nuclei form at random in the whole volume, their initial volume is considered nil and their location is fixed in space (diffusion of nuclei does not occur). Once a nucleus is formed it starts growing, its size increases and upon collision with other nuclei the growth ceases at the common interface, according to the impingement mechanism. The growth law of the nucleus, that is the time dependence of the nucleus radius, is assumed to be known and it is usually in the form of a power of time, $R \propto t^m$ ($m \geq 1$). The KJMA mean-field theory provides the temporal evolution of the volume of the new phase and of the mean volume of crystals [18].

The KJMA model is an application of Poisson statistics to the nucleation process, since the spatial distribution of nucleation centres is assumed random throughout the whole space. In this case, the exact solution of the phase transformation kinetics is given by simple analytical expressions, useful for interpreting experimental data [11,18,19]. A key equation of the KJMA theory links the rate of formation of the *actual* nuclei (i.e. measured in experiment), $I_a(t)$, to the nucleation rate throughout the whole space $I_0(t)$ (i.e. by also including the so-called phantom nuclei) [18]:

$$I_a(t) = I_0(t)(1 - \xi(t)) \tag{1}$$

with $\xi(t)$ being the volume fraction of the transformed phase at time t. Alternatively, $\xi(t)$ is the excluded volume for nucleation. As stated above, application of Poisson statistics requires the complete randomness of the system, that is the distribution of nuclei must be random throughout the whole space. In the mathematical formulation of the kinetics, this implies nucleation even in the transformed phase (phantom nuclei) [20]. In eqn.1, $I_a(t)$ is the number of actual nuclei that start growing in unit time divided by the total volume of the system. Consequently, $I_0(t)$ is equal to the rate of formation of actual nuclei per unit of *untransformed* volume. In practical application of the model, $I_0(t)$ is usually a simple function given *a priori* (with constant or exponential behavior) although it can be in principle computed employing kinetic theories of nucleation stage [3,21].

However, in several systems the Poissonian distribution of nuclei is the exception rather than the rule, especially in transformations in the solid state [4,5]. A paradigmatic example is the electrodeposition of a new phase on solid substrate driven by progressive nucleation, where the spatial distribution of nuclei is not random [22–25]. This is due to the diffusion fields around growing nuclei implying a reduction of supersaturation and, consequently, of the nucleation probability around the already formed nuclei [26–28]. It stems that around each nucleus there is a depletion region where nucleation is drastically reduced [22]. In other words, within a distance, say R_{hc} from nuclei centres, nucleation is suppressed while proceeds at the same rate everywhere out of these regions (approximation of uniformity of metastable phase [29]). It follows that the next neighbour nucleus cannot lie at a distance shorter than the correlation radius, R_{hc}. In this context, it is worth quoting the paper by Grinin et al on a statistical model for the nucleation probability of a nearest droplet to an already formed one, in supersaturated vapor condensation [29]. In a shell around the nucleus - the

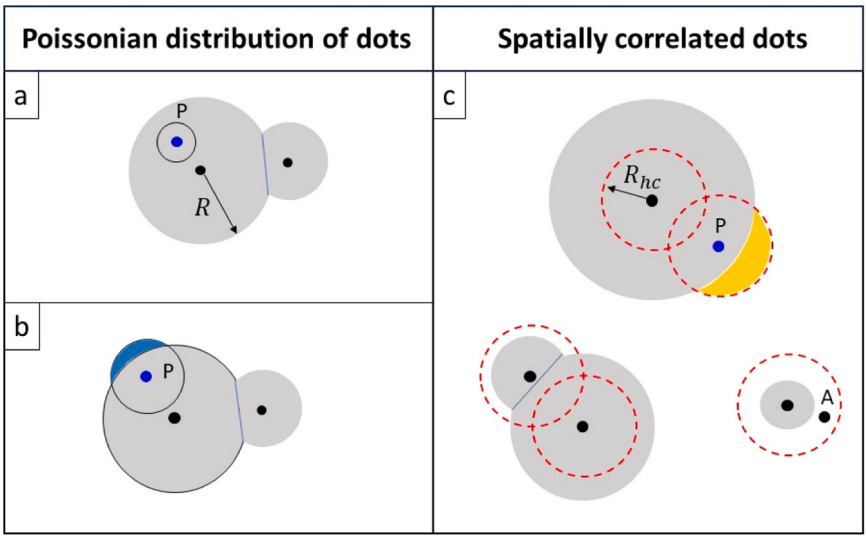

Fig. 1. Pictorial view of an arrangement of dots (nuclei centres, black points) in phase transformation ruled by progressive nucleation and growth with impingement. In the figure, the blue dot, *P*, is a phantom, *R* is the nucleus radius and R_{hc} the correlation disk. Panel *a*) shows two actual nuclei and a phantom nucleus within the transformed phase. In the case of KJMA compliant growth (e.g. linear growth and random nucleation) the overgrowth phenomenon is precluded and the KJMA kinetics applies. Phantom overgrowth occurs for parabolic growth law, as depicted in panel *b*) (blue area of the phantom nucleus), where the KJMA kinetics does not hold for $\xi(t)$. However, in both cases of panels *a*) and *b*) the actual nucleation rate is given by Eq.1 Panel *c*): non-random nucleation according to the hard-disk correlation. In the figure, the dashed red circle is the correlation disk, within which nucleation is suppressed. At odds with the KJMA model, considering phantoms will alter the stochastic process, since nucleation could be precluded even where it should be allowed. This is the region coloured in yellow within the correlation disk of the phantom. Nucleation can be also precluded in the uncovered portion of the surface, namely within the correlation disk of an actual nucleus (for instance in point A). In this case Eq.1 does not hold.

Knudsen layer - the nucleation rate is strongly reduced and increases with the distance from the central droplet [29]. Kuchma et al [30] have also investigated the effect on nucleation rate of local depletion of supersaturation due to the formation of gas bubbles in decompressed fluid. The authors developed a mean-field theory for the nucleation stage and introduce the concept of excluded volume in which the generation of new gas bubbles is suppressed, owing to the decrease of supersaturation of the dissolved gases. The model deals with multicomponent systems and allows one to estimate the size distribution function of bubbles as the image of nucleation rate in terms of the birth times of the bubbles and nucleus growth law [30].

Another process, important for technological application, is the growth of diamond film by seeding of the substrate surface with diamond nuclei [31,32]. Due to the finite size of the seeds, the formation of the diamond phase occurs by site-saturated nucleation, growth with impingement and hard-disk correlation between nuclei. Theoretical modeling with application to experimental data are reported in ref.[32]. It is worth stressing that, with respect to the spatial correlation between nuclei, the two types of systems discussed so far are different, since in the first the correlation radius is a function of time while in the case of seeding, and in nucleation at pre-existing sites as well, can be taken as constant.

During the last years, to extend the range of applicability of the KJMA theory, approaches have been formulated for describing phase transformation kinetics with correlated nuclei [33–36]. These modelling make use of the *n*-dots correlation functions for computing the probability that no dot is located within a given region of space. The theory has been applied to phase transitions with site-saturated nucleation [33,34,37] and generalized to the case of progressive nucleation in refs.[35,38]. At odds with the KJMA model, in the case of progressive nucleation of spatially correlated nuclei, the mathematical solution of the kinetics is expressed in terms of the actual nucleation rate, I_a, rather than that including phantoms, I_0 [39]. The model case of transformations with correlated nuclei and constant value of I_a has been discussed in ref.[38]. A more realistic approach would require computing the actual nucleation rate as a function of the degree of advancement of the transformation, namely the time. Because of the correlation constraint, in transformations with correlated nuclei eqn.1 does not hold, in general, since nucleation could be inhibited even in the untransformed volume. This point is made clear through Fig. 1 which illustrates the case of progressive nucleation in 2D for both random distribution of nuclei (panels *a*, *b*) and for nuclei with hard-disk correlation (panel *c*). As displayed in panel *c*), the hard-disk correlation prevents nucleation even in the untransformed portions of the surface.

Eqn.1 holds true also for the parabolic growth law ($R \propto t^{1/2}$), although such a growth mode is non-compliant with the KJMA approach owing to the overgrowth of phantoms [20]. In this case the volume fraction is not given by the usual KJMA kinetics [40,41]. In fact, the computation of $\xi(t)$ for random nucleation and parabolic growth requires employing, in the stochastic approach, the actual nucleation rate given by eqn.1 and the correlation functions [42,43].

The aim of the present work is to model the nucleation rate of actual nuclei in phase transformations that meet the KJMA assumptions above reported, apart from the randomness condition that is removed. As in the KJMA approach the I_0 quantity is given a priori and will be taken constant. As far as the correlation is concerned, hard-sphere interaction is considered, i.e. the distance between the centres of a pair of nuclei cannot be shorter than a given value, R_{hc}. In case of constant R_{hc}, as considered in the present contribution, the arrangement of nuclei centres resembles those of the centres of an ensemble of hard-spheres with diameter R_{hc}. Besides, a fluid of hard-spheres, whose pair interaction potential determines the correlation function, provides the simplest model of a liquid. Accordingly, the terms hard-sphere interaction, hard-sphere correlation and hard-core interaction are in use.

The hard-core correlation discussed in the present paper can be due to several mechanisms such as:

i) Nucleation at preferential sites [4, 32]; ii) The formation of interacting dipole moments upon nucleating particles [44,45]; iii) In the Stranski-Krastanov mechanism, the effect of stress/strain can lead to repulsive interaction in analogy with the electric dipoles [44, 46].

Recently, non-random nucleation with hard-core interaction has been experimentally observed by Rost et al [44] in the electrochemical oxidation of Pt(111). Based on the experimental determination of nucleus-nucleus correlation function by STM (Scanning Tunneling Microscopy) and computations on the energetics of the system, the authors demonstrate that the hard-disk correlation is given by nucleation at preferred sites that are created, during the early stage of oxidation, by repulsive interaction of precursors (the place exchange atoms) [44].

The paper is divided as follows: in Section 2.1 we outline the stochastic approach for correlated nucleation that is employed, in Section 2.2, for modelling nucleation rate in progressive nucleation in two- and three-dimensional space. The outputs of the numerical computation are discussed in Section 2.3. To make the presentation of the subject matter easer to follow, most of the mathematical derivations are reported in the Appendix and in the Supplementary Material sections.

2. Results and discussion

2.1. Phase transformations with spatially correlated nuclei

The stochastic approaches for modeling the kinetics of phase transformations by nucleation and growth rest on the determination of the probability that no dots (i.e. the centers of nuclei) lie within a given volume centered at a generic point of space. In kinetics with site saturated nucleation and spherical nuclei the measure of this region, $|\Delta_t|$, is the volume of the nucleus at time *t*: $|\Delta_t| = \int_{\Delta_t} d\boldsymbol{r}$. From this probability the volume fraction of the transformed phase is obtained according to, $\xi(t) = 1 - Q_0(\Delta_t)$ where $Q_0(\Delta_t)$ is the probability that no dots are within the sphere Δ_t centered at a generic point of the space. In fact, the absence of any nucleus in a sphere of radius equal to the nucleus radius, at *t*, guarantees that the center of this sphere is not within any nucleus at that time, i.e. the generic point of the space does not belong to the new phase at *t*. For a random distribution of *N* dots per unit volume, the Poisson distribution gives

$Q_0(\Delta_t) = e^{-N|\Delta_t|}$, that leads to the KJMA kinetics [18]. In the case of spatially correlated nuclei with site-saturated nucleation, the above probability is given in terms of a series of correlation functions. Truncation of the series up to the second order term provides [33,34]

$$Q_0(\Delta_t) = \exp\left[-N|\Delta_t| + \frac{1}{2}N^2 \int_{\Delta_t} d\boldsymbol{r}_1 \int_{\Delta_t} d\boldsymbol{r}_2 g_2(\boldsymbol{r}_1, \boldsymbol{r}_2) \right], \tag{2}$$

where g_2 is the 2-dots correlation function that is related to the pair distribution function, $g(\boldsymbol{r}_1, \boldsymbol{r}_2)$, through the expression $g_2(\boldsymbol{r}_1, \boldsymbol{r}_2) = g(\boldsymbol{r}_1, \boldsymbol{r}_2) - 1$. For homogeneous systems, translationally invariant as considered here, $g(\boldsymbol{r}_1, \boldsymbol{r}_2) = \quad g(|\boldsymbol{r}_1 - \boldsymbol{r}_2|) = g(r)$.

Eq.2 has been generalized to the case of progressive nucleation implying, at any time, a distribution of nucleus size. In the following, we refer to the nucleus center as dot. We consider a set of distinguishable classes of dots. Within each class dots are indistinguishable. Since nuclei start growing at different times, the growth law now depends on both actual time, t, and birth time, t', of the nuclei. The classes of dots are labelled with the nucleus birth times to which, in this case, the correlation function may also depend. For instance, the correlation function of a couple of nuclei with birth times t_1 and t_2 reads $g_2(\boldsymbol{r}_1, \boldsymbol{r}_2, t_1, t_2)$. Employing the same order of approximation of Eq.2, the probability that no dots of the "t'-*class*" is located within the domain $\Delta_{t',t}$, for any t' in the range $0 < t' < t$, becomes [38] (see also Appendix A)

$$Q_0(\Delta_{0,t}) =$$

$$\exp\left[-\int_0^t I_a(t')|\Delta_{t',t}|dt' + \int_0^t I_a(t_1)dt_1 \int_0^{t_1} I_a(t_2)dt_2 \int_{\Delta_{t_1,t}} d\boldsymbol{r}_1 \int_{\Delta_{t_2,t}} d\boldsymbol{r}_2 g_2(\boldsymbol{r}_1, \boldsymbol{r}_2, t_1, t_2) \right], \tag{3}$$

where $I_a(t')$ is the nucleation rate of actual nuclei at time t' and $\Delta_{0,t}$ stands for the whole sequence of the $\Delta_{t',t}$ domains. The volume fraction of the transformed phase is given by Eq.3 by considering for $\Delta_{t',t}$ the sphere with radius equal to the nucleus radius at t. In fact, by denoting with $R(t,t') \equiv R(t-t')$ the radius of the nucleus, we get $|\Delta_{t',t}| = \int_{\Delta_{t',t}} d\boldsymbol{r} = \nu_D R(t,t')^D$ with D space dimension and ν_D a geometrical factor ($\nu_2 = \pi$, $\nu_3 = 4\pi/3$). In other words, $Q_0(\Delta_{0,t})$ is the probability that the centre of the nuclus born in time interval $0 < t' < t$ does not belong to a sphere of radius $R(t,t')$ centered at a generic point of the space. It follows that $Q_0(\Delta_{0,t})$ is the probability that a generic point of space does not belong to the new phase, from which the volume fraction is obtained: $\xi(t) = 1 - Q_0(\Delta_{0,t})$.[1]

When $I_a(t')$ is given by eqn.1, Eq.3 provides an integral equation for ξ or, equivalently, for $\frac{I_a(t')}{I_0} = Q_0(\Delta_{0,t'})$. In this case, the distribution of dots is random through the space, yet correlation is present between the *actual nuclei*. In fact, the relative distance between two nuclei, born at t_1 and t_2, must satisfy the constraint $r > R(t_1 - t_2)$ for nucleus 1 not to be a phantom [43]. Therefore, the radial distribution function is nil for $r < R(t_1 - t_2)$ which implies spatial correlation among actual nuclei in KJMA compliant growths. This point is further discussed in Section 2.2. Eq.3 was employed in refs.[39,43] for studying phase transformations with growth law of the diffusion-type.

2.2. Nucleation rate of actual nuclei

As anticipated in the introduction, Eq.2 holds whenever nuclei form at random in the untransformed portion of the volume. However, as illustrated in Fig. 1c, spatial correlation among nuclei may prevent nucleation even in the untransformed phase, for which Eq.1 is invalid. The computation of $I_a(t)$ is more involved, in this case, since it requires tackling a different stochastic process than the one for the $\xi(t)$ function (Eq.3).

In the following, this topic is studied for the hard-sphere interaction between actual nuclei where, at the lowest order, the pair distribution function of dots is equal to $g(r) \cong H(r - R_{hc})$, with $H(\bullet)$ the Heaviside step function and R_{hc} the correlation radius. In fact, higher order terms in the series expansion of the $g(r)$ can be neglected for low densities of nuclei. The validity of this approximation in phase transformations has been discussed in ref.[33]. However, the $g(r)$ above reported only holds for nucleation that could occur within the correlation sphere of another nucleus. In fact, given two nuclei with birth times t_1 and t_2 (where $t_2 < t_1$ is considered) the conditions according to which both their distance is greater than R_{hc} and the first nucleus is not a phantom, requires the constraints $r > R_{hc}$ and $r > R(t_1 - t_2)$ to be satisfied. Consequently, the pair distribution function is given by:

$$g(r, t_1, t_2) = \begin{cases} H(r - R_{hc}), & \text{for } R(t_1 - t_2) < R_{hc} \\ H(r - R(t_1 - t_2)), & \text{for } R(t_1 - t_2) > R_{hc}, \end{cases} \tag{4}$$

where $|\boldsymbol{r}_1 - \boldsymbol{r}_2| = r$ is the relative distance between the couple of nuclei with birth time t_1 and t_2. In compact form Eq.4 reads $g(r, t_1, t_2) = H(r - R_{hc})H(r - R(t_1 - t_2))$.

The stochastic process for computing I_a can be envisaged according to the following: between time t and $t + \Delta t$, $I_0 \Delta t$ dots, distributed at random in the whole volume, start growing with an exception of the dots, located either within the new phase or closer to

[1] In the case of thin film growth at solid surfaces, the computation provides the substrate coverage by the film ($D = 2$), where for spherical-cup particles $\nu_2 = \pi$.

another nucleus than R_{hc}, that are removed from the system. The rate of formation of the actual nuclei is therefore given by

$$I_a(t) = I_0 Q_a(t), \tag{5}$$

where Q_a is the probability that a generic point of the system does not belong to the new phase and its distance from next neighbour nuclei exceed R_{hc} .[2] This probability is computed by means of Eq.3 with a judicious choice of the $\Delta_{t',t}$ integration domain. We recall that Eq.3 provides the probability that no dot lies in this domain: in fact, in the $g(r)$ containing term, the $\Delta_{t_1,t}$ and $\Delta_{t_2,t}$ refer to the exclusion of dots 1 and 2, respectively, from these domains (see also Appendix A). In the following, we consider linear growth of nuclei, $R(t,t') = a(t-t')$ with a the growth rate. To determine the $\Delta_{t',t}$ domain we define the time t^* from the equation $R(t,t^*) = R_{hc}$, namely $t^*(t) = t - \frac{R_{hc}}{a}$ at running time t. For $t > \frac{R_{hc}}{a}$ the time t^* defines two populations of nuclei with sizes greater and shorter than the correlation radius, R_{hc}. This is shown in Fig. 2 where the growth law is plotted as a function of running time and for several values of the birth time, t', in the interval $(0,t)$. Based on this, for the present stochastic process the radius of the spherical domain $\Delta_{t',t}$ is

$$r(t,t') = [R_{hc}H(t'-t^*) + R(t,t')H(t^*-t')]H\left(t - \frac{R_{hc}}{a}\right) + R_{hc}H\left(\frac{R_{hc}}{a} - t\right), \tag{6}$$

that will be employed in Eq.3 for transformations in both 2D and 3D space.

The pair distribution function Eq.4 depends on both the birth times of the couple of nuclei, t_1 and t_2 (where $t_2 < t_1$ and $R(t,t_2) > R(t,t_1)$) and on the size of the second nucleus at the birth time of the first, $R(t_1,t_2) = R(t_1 - t_2)$. According to Eq.6 the following cases are considered ($t^* > 0$ i.e. $t > \frac{R_{hc}}{a}$):

a- for $R(t_1 - t_2) < R_{hc}$:

$$\text{i) } t* < t_2 < t_1,\ r(t,t_1) = r(t,t_2) = R_{hc}; \tag{7a}$$

$$\text{ii) } t_2 < t* < t_1,\ r(t,t_1) = R_{hc},\ r(t,t_2) = R(t,\ t_2); \tag{7b}$$

$$\text{iii) } t_2 < t_1 < t*,\ r(t,t_1) = R(t,t_1),\ r(t,t_2) = R(t,\ t_2). \tag{7c}$$

b- for $R(t_1 - t_2) > R_{hc}$:

the cases ii) and iii) above still hold whereas case i) does not. In fact, case i) implies

$t_1 - t_2 < t - t^*$ and $a(t_1 - t_2) = R(t_1 - t_2) < a(t - t^*) = R_{hc}$, that is incompatible with the constraint $R(t_1 - t_2) > R_{hc}$.

For $t < \frac{R_{hc}}{a}$ all growing nuclei are within the correlation sphere and the stochastic problem of finding $Q_a(t)$ is equivalent to that of the Random Sequential Adsorption (RSA), for the random packing of spheres of diameter R_{hc} in D-dimensional space [47–49]. This point is further discussed in the next section.

As regards the spatial integral over the correlation function entering Eq.3, it can be simplified using polar or spherical coordinates. Since the system is homogeneous, we get:

$$\psi(t,t_1,t_2) = \int_{\Delta_{t_1,t}} d\boldsymbol{r}_1 \int_{\Delta_{t_2,t}} d\boldsymbol{r}_2 g_2(\boldsymbol{r}_1,\boldsymbol{r}_2,t_1,t_2) = \Omega_D \int_0^{r(t_1,t)} r_1^{D-1} dr_1 \int_{\Delta_{t_2,t}} d\boldsymbol{r}_2 g_2(r,t_1,t_2), \tag{8}$$

where Ω_D is the solid angle ($\Omega_3 = 4\pi$) or the polar angle ($\Omega_2 = 2\pi$) and $r = |\boldsymbol{r}_1 - \boldsymbol{r}_2|$ the relative distance. Since $g_2(r,t_1,t_2) = g(r,t_1,t_2) - 1$, the integral provides two second order terms, i.e. due to the Heaviside function and to the -1 constant. As reported in details in the Supplementary Material (section S1), the integral with the Heaviside function can be expressed in terms of the overlap volume of two spheres of radius $R(t,\ t_2)$ and R_{hc}, for $R(t_1 - t_2) < R_{hc}$, and of radius $R(t,\ t_2)$ and $R(t_1 - t_2)$ for $R(t_1 - t_2) > R_{hc}$. In Eq.8 the second order contribution due to the term -1 is equal to $-|\Delta_{t_1,t}||\Delta_{t_2,t}|$. Finally, the $\psi(t,t_1,t_2)$ function (Eq.8) is integrated with the actual nucleation rate over the time variables t_1 and t_2. Fig. 3 shows the integration domains of the double integral in time, for the cases i)-iii) of eqn.7a-c. In the figure, the different colors highlight that for these cases the spatial integrals, $\psi(t,t_1,t_2)$, are in general different. The straight line, in red, is the equation $t_2 = t_1 - \frac{R_{hc}}{a}$ (i.e. $R(t_1 - t_2) = R_{hc}$) at the boundary between conditions $R(t_1 - t_2) < R_{hc}$ and $R(t_1 - t_2) > R_{hc}$ whose domains are above and below this line, respectively. For $t < \frac{R_{hc}}{a}$ the red line shifts to the dashed blue one and only the condition $R(t_1 - t_2) < R_{hc}$ holds true. This is equivalent to the RSA. Moreover, for $R_{hc} = 0$, the KJMA model is recovered, and the integration domain is that for case iii) with $R(t_1 - t_2) > R_{hc}$ (white colored domain in Fig. 3). However, because of the correlation between actual nuclei Eq.8 is different from zero even for $R_{hc} = 0$. Details on the computation of these integrals are reported in Supplementary Material (sections S1, S2).

2.3. Numerical computation of the nucleation rate actual and volume fraction

This section is devoted to the numerical computation of both nucleation kinetics and volume fraction of the new phase for 2D and

[2] $[1 - Q_a(t)]$ is the fraction of volume excluded to nucleation.

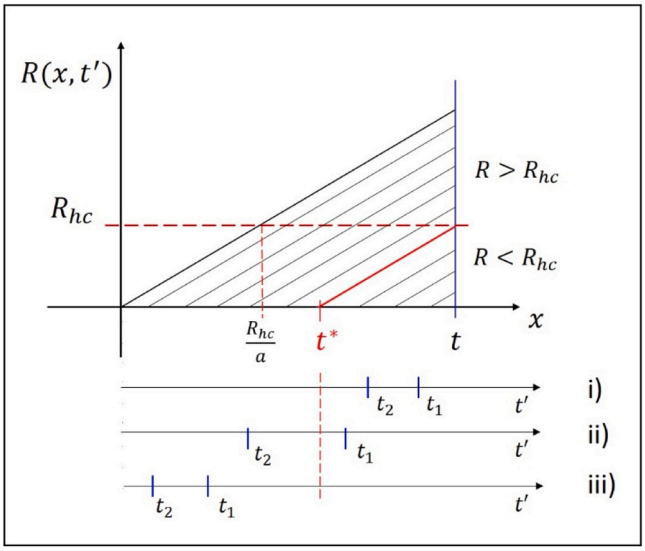

Fig. 2. Linear growth of nuclei for several values of the birth time, t', in the range $0 < t' < t$. The growth law is $R(x,t') = a(x - t')$ with $x \geq t'$. At running time $t > \frac{R_{hc}}{a}$ two sets of nuclei are defined, with $R > R_{hc}$ and $R < R_{hc}$, namely with birth time shorter or larger that $t^*(t) = t - \frac{R_{hc}}{a}$. The figure also displays the birth times of the couple of nuclei considered in the second order contribution of the probability function, i.e. the cases i)-iii) of Eqs.7a-c. At time $t < \frac{R_{hc}}{a}$ there is just one set of nuclei with $R < R_{hc}$ and the stochastic process is the same as the RSA.

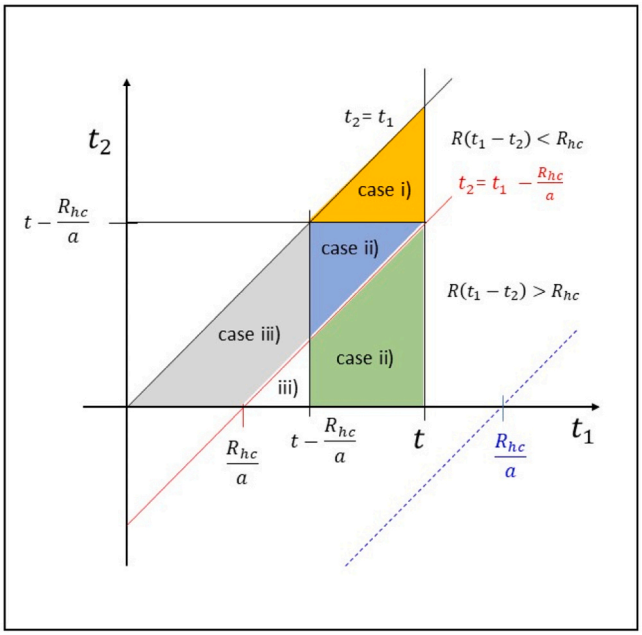

Fig. 3. Integration domains of the time integral according to the constraints reported in Eqs.7a-c. Since $t_1 > t_2$, the integration domain is below the line $t_2 = t_1$. Similarly, the conditions $R(t_1 - t_2) < R_{hc}$ and $R(t_1 - t_2) > R_{hc}$ are satisfied above and below the red line $t_2 = t_1 - \frac{R_{hc}}{a}$, respectively. The different colors of the domains imply different time-functions resulting from the space integral. The graph shows the case $t > \frac{R_{hc}}{a}$ when the maximum size is greater than the correlation sphere. For the case $t < \frac{R_{hc}}{a}$ the equation $t_2 = t_1 - \frac{R_{hc}}{a}$ is displayed as dashed blue line. The condition $R(t - t') > R_{hc}$ is not satisfied and the stochastic process for determining Q_a is the same as the RSA.

3D transformations. The numerical computations have been carried out using the Wolfram Mathematica package.

The rate of formation of actual nuclei is computed through Eqs.3,4 with the integration domains reported in eqns.7a-c and in Fig. 3. Use of Eq.3 in Eq.5 results in an integral equation for $I_a(t)$. From the knowledge of $I_a(t)$ it is possible to determine the volume fraction of the transformed phase through Eq.3, in which $\left|\Delta_{t',t}\right| = \frac{\Omega_D}{D} R(t,t')^D$ is the nucleus volume [38]. In the computation, we used reduced

quantities where lengths are normalized to the maximum size of the nucleus, $R(t,0) = at$. In the case of linear growth, as considered here, we define $\rho_{hc} = \frac{R_{hc}}{at}$ and the reduced time $\tau^* = \frac{t^*}{t} = 1 - \rho_{hc}$ for $\rho_{hc} < 1$. With the same normalization the growth law becomes $\rho(\tau_i) = \frac{a(t-t_i)}{at} = 1 - \tau_i$ (with $i = 1, 2$) and the r_1 variable changes in $x_1 = \frac{r_1}{at}$. The rate I_0 is constant and, in analogy with the KJMA kinetics, the extended volume is given by [3] $X_{ex}(t) = \frac{\Omega_D}{D(D+1)} I_0 a^D t^{D+1} = \left(\frac{t}{\bar{\tau}_D}\right)^{D+1}$, namely $V_{ex} = \left(\frac{t}{\bar{\tau}_3}\right)^4$ and $S_{ex} = \left(\frac{t}{\bar{\tau}_2}\right)^3$, respectively for transformations in 3D and 2D. In terms of reduced time, $\bar{t} = \frac{t}{\bar{\tau}_D}$, one gets $\rho_{hc} = \frac{1}{\bar{t}}\left(\frac{\gamma}{3}\right)^{1/(D+1)}$ where $\gamma = 3R_{hc}^{D+1}\frac{\Omega_D}{D(D+1)}\frac{I_0}{a} = R_{hc}^{D+1}\frac{\pi I_0}{a}$ is a measure of the degree of correlation between nuclei. For the KJMA model $\gamma = 0$.$\gamma = 3R_{hc}^{D+1}\frac{\Omega_D}{D(D+1)}\frac{I_0}{a} = R_{hc}^{D+1}\frac{\pi I_0}{a}$ is a measure of the degree of correlation between nuclei. For the KJMA model $\gamma = 0$.

Eqs.3–5 provide the following integral equation for $Q_a(\tau)$,

$$Q_a(\bar{t}) = \exp(F[Q_a]), \tag{9}$$

where $F[Q_a]$ denotes the functional of the Q_a probability function reported in Eq.B1 in Appendix A (see also section S3 in Supplementary Material).

To test the validity of the present approach, we first apply Eq.9 to KJMA compliant transformations for which $Q_a(\bar{t})$ is given by Eq.1 according to $Q_a(\bar{t}) = e^{-X_{ex}(\bar{t})} = e^{-(\bar{t})^{D+1}}$. Specifically, $F[Q_a]$ (Eq.B1 in Appendix A) has been computed, as a function of $\bar{t}$, at $\rho_{hc} = 0$ by using $\tau_i = \frac{t_i}{t}$ $(i = 1, 2)$ as integration variables and $Q_a(\tau_i) = \exp\left[-\left(\frac{t\tau_i}{\bar{\tau}_D}\right)^{D+1}\right] = \exp\left[-(\tau_i)^{D+1} X_{ex}(\bar{t})\right]$.[4] Next, the computation has been compared with the solution of the KJMA theory to check the validity of Eq.9, namely to verify the identity $e^{-(\bar{t})^{D+1}} = \exp\left(F[\exp\left(-(\tau)^{D+1} X_{ex}(\bar{t})\right)]\right)$.

As displayed in Fig. 4, there is a very good agreement between the exact solution and the actual nucleation rate, Eq.3, for 3D and 2D transformations. In the case of spatially correlated nuclei, Eq.9 has been solved numerically by successive iterations and for several values of $\bar{t}$: $Q_a^{(k)} = \exp\left(F[Q_a^{(k-1)}]\right)$, with $k \geq 1$ number of iterations. For the function $Q_a^{(0)}$ we have chosen the KJMA solution: $Q_a^{(0)}(\bar{t}) = e^{-X_{ex}(\bar{t})}$. In general, with about 10 iterations the relative integral error is of the order of 0.02 % at the highest correlation value investigated here. Typical behavior of the error with the number of iterations is reported in the Appendix A (Fig.B1). This result and those of Fig. 4 suggest that the convergence of the integral equation is affected by the γ parameter. In fact, since for $\gamma = 0$ the convergence is nearly achieved with no iterations, we expect that the smaller γ the faster the convergence by successive iterations. Noteworthy, we get a single parameter for the convergence behavior with iteration number, which depends on all physical quantities that rule the phase transformation.

The time dependence of the actual nucleation rate is displayed in Fig. 5 for several values of γ. The hard-sphere correlation imparts a change in the curvature of the $\frac{I_a}{I_0}$ vs $\bar{t}$ function in the initial portion of the kinetics that is wider the higher γ. In fact, the initial behavior of the function resembles the RSA kinetics up to $t_{hc} = \frac{R_{hc}}{a}$, i.e. $\rho_{hc} = 1$, from which $\bar{t}_{hc} = \left(\frac{\gamma}{3}\right)^{1/(D+1)}$. This value is close to the first inflection point of the curves of Fig. 5a that occur at $\bar{t} = 0.3,\ 0.6,\ 0.7,\ 0.85$ and 0.95 with increasing γ, in fair agreement with the values $\bar{t}_{hc}$= 0.36, 0.64, 0.76, 0.9 and 1.0. For the curves in Fig. 5b the inflection points are at $\bar{t} = 0.2,\ 0.52,\ 0.67$ and 0.92 in fair agreement with the values $\bar{t}_{hc}$= 0.25, 0.55, 0.69 and 0.92. After these times, the curves get closer to the KJMA kinetics the lower γ and eventually merge to the tail of the Poissonian curve.

Fig. 6 displays the density of actual nuclei with time for the dimensionless quantity $N(\bar{t}) = \left(\frac{a}{I_0}\right)^{D/(D+1)} n_a(\bar{t})$, where $n_a(\bar{t}) = I_0 t(\bar{t}) \int_0^1 Q_a(\tau) d\tau$. The number density of nuclei increases with time, monotonically, to reach the asymptotic value that is higher the lower the correlation radius (i.e. γ).

The number density of nuclei is further employed to compare the nucleation rate with that of the RSA process of spheres with diameter R_{hc}. Let us consider the RSA process at time t, when $n_a(t)$ spheres have been placed into the system. At time t the adsorption rate is given by $\frac{dn_a(t)}{dt} = I_0 Q_0(\Delta_{RSA}, n_a(t))$, where Δ_{RSA} is a sphere of radius R_{hc} [47,48] and $Q_0(\Delta_{RSA}, n_a(t))$ the probability that no center of the $n_a(t)$ spheres is found within Δ_{RSA}. Accordingly, to determine $Q_0(\Delta_{RSA}, n_a(t))$ we apply Eq.2 for the site-saturated nucleation with time dependent $N \equiv n_a(t)$.

The kinetics of RSA is studied as a function of the volume fraction that is occupied by the non-overlapping spheres, namely $\theta(t) = \frac{\Omega_D}{D}\left(\frac{R_{hc}}{2}\right)^D n_a(t)$. It is worth recalling that Eq.2 is suitable to study adsorption kinetics, although it does not provide the exact value of the packing at the jamming point, θ_c [33,48]. In fact, $Q_0(\Delta_{RSA})$ must be zero for $\theta \geq \theta_c$, a condition that is not satisfied by the functional form of Eq.2 that approaches zero, asymptotically.

[3] For constant nucleation rate, I_0 (with the inclusion of phantoms), the extended volume is defined as:$X_{ex} = I_0 \int_0^t v(t,t')dt'$, where $v(t,t')$ is the nucleus volume.

[4] To simplify the notation, we retain the same symbol for either $Q_a(\tau_i)$ and $Q_a(t_i)$ functions, as well as in similar occurrences in the text.

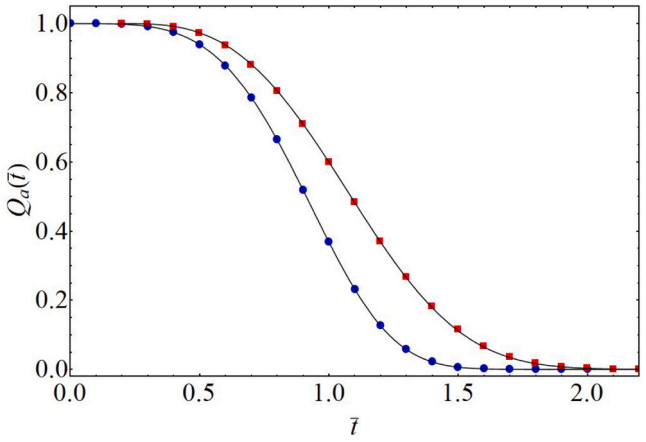

Fig. 4. Exact analytical solution of the kinetics for random distribution of nuclei according to eqn.1 and the KJMA theory: $Q_a = \exp\left[-(\bar{t})^{D+1}\right]$ (solid lines for $D = 2$ and $D = 3$). The plot also shows the kinetics computed by the right-hand side of Eq.9 at $\gamma = 0$, with Q_a given by the KJMA solution above reported (symbols). Solid circles and solid squares refer to transformations in 3D and 2D, respectively. The kinetics at $D = 2$ has been shifted by $\Delta\bar{t}$= 0.2. The integral error is about 0.04 % and 0.3 % for 3*D* and 2*D* transitions, respectively. The very good agreement between the two sets of data gives support to the second order approximation employed in the computation.

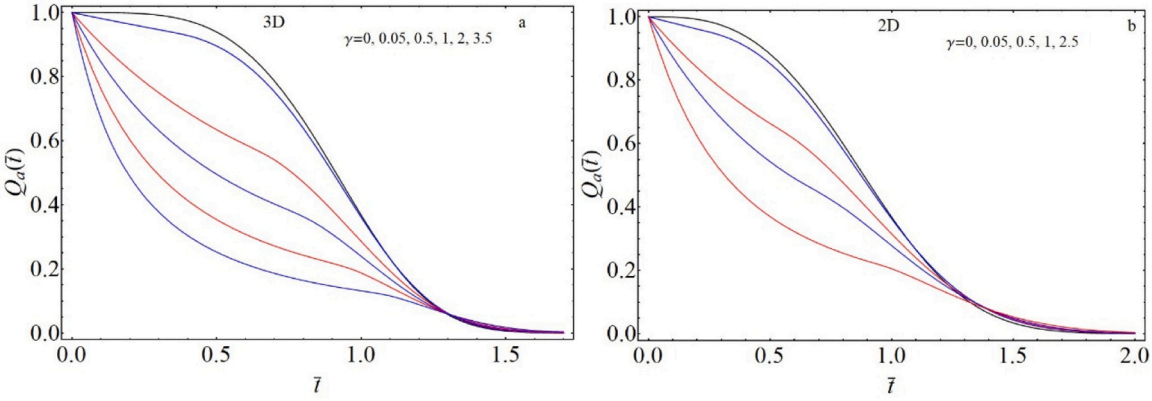

Fig. 5. The nucleation rate, $Q_a = \frac{I_a}{I_0}$, is displayed as a function of reduced time, $\bar{t}$, for several values of γ for 3D (panel *a*) and 2D (panel *b*) transformations. The correlation degree, γ, increases along the set of curves from top to bottom.

From Eq.2 the RSA kinetics is given by

$$Q_{RSA}(\theta) = \exp\left[-2^D\theta\left(1+2^{D-1}\theta\right)+\frac{D^2 2^{2D-1}}{\Omega_D}\theta^2\beta_D\right], \tag{10}$$

where $\beta_3 = \frac{17\pi}{72}$ and $\beta_2 = \frac{3\sqrt{3}}{8}$ are related to the mean value of the overlap volume of two spheres of unitary radius (for details, see section S4 in Supplementary Material). The comparison between the actual nucleation rate in phase transformations with correlated nuclei and the rate of RSA is displayed in Fig. 7. In the figure, the probabilities Q_{RSA} and Q_a are plotted as a function of θ, namely the total volume occupied by the adsorbed spheres of radius $\frac{R_{hc}}{2}$. In Fig. 7 the dotted line is the RSA kinetics Eq.10 and the solid line the nucleation rate of the phase transformation. The kinetics do show that the nucleation rate coincides with the rate of the RSA up to the value $Q_a(\theta(\bar{t}_{hc}))$ marked on the Q_a-axis. Beyond this point, the growth process mainly rules the kinetics, and the shape of the curve becomes like the KJMA one, which is the nearly vertical line in Fig. 7 (parallel to the Q_a-axis). In fact, for $R_{hc} = 0$, θ is identically nil. In panel *a*) it is also reported the behavior of the volume fraction with θ, for two values of γ. It stems that the transformation reaches completion for $\bar{t}\to\infty$, $Q_a\to 0$ and $\theta\to\theta(\infty) = n_a(\infty)\frac{\Omega_D}{D}\left(\frac{R_{hc}}{2}\right)^D$, where $n_a(\infty)$ is the number density at saturation (Fig. 6). Fig. 7 also shows that, although the number density of nuclei at saturation decreases with γ, $\theta(\infty)$ increases with correlation radius and its value is always lower than the value at the jamming point. This is due to the growth process because adsorption of the spheres is not allowed in the new phase.

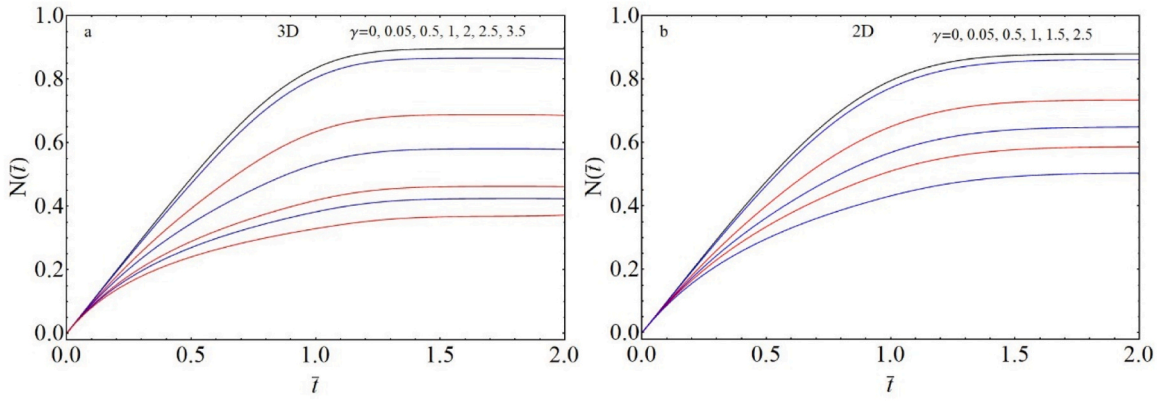

Fig. 6. Number density of actual nuclei as a function of reduced time, $\bar{t}$, and correlation degree (γ) for 3D and 2D transitions (panels *a* and *b*). The number density is normalized to the quantity $\left(\frac{I_0}{a}\right)^{D/(D+1)}$. In both panels the normalized number density of nuclei at saturation decreases with increasing γ.

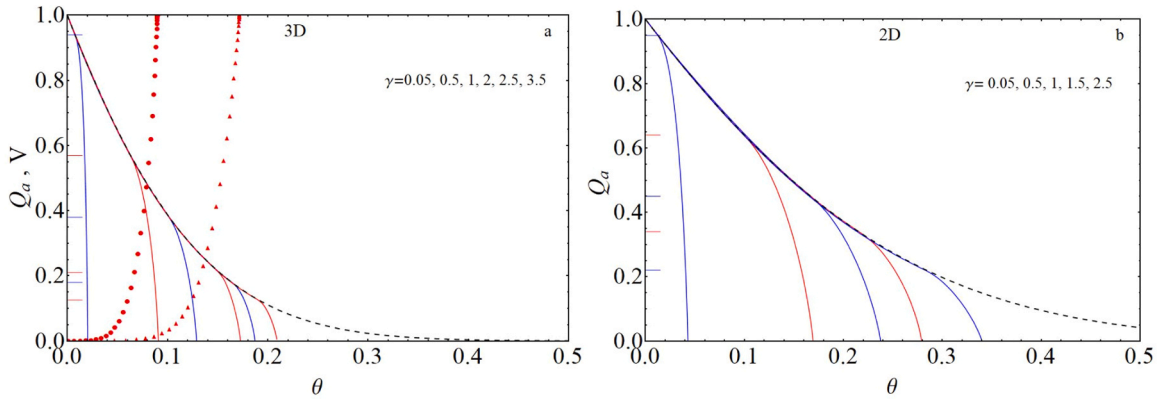

Fig. 7. Comparison between the kinetics of nucleation in phase transformation with hard-core correlation and RSA, for 3D (panel *a*) and 2D (panel *b*) transformations. The dashed line is the RSA kinetics computed through Eq.10, where θ is the fraction of volume that is occupied by the spheres of diameter R_{hc}. In the curves, the γ value increases from left to right. The kinetics follow the RSA curve up to time $\bar{t}_{hc}$ when $\rho_{hc} = 1$. At this point, the growth of nuclei rules the kinetics that deviate from the RSA curve. The transition points are marked on the Q_a axis for the various curves. After these points, the kinetics become like the KJMA behavior that is the vertical line parallel to the Q_a axis. Panel *a*) also shows the behavior of the volume fraction, $V(\theta)$, for $\gamma = 0.5$ and $\gamma = 2$ (symbols). The asymptotic values, $\theta(\infty)$, correspond to zero nucleation rate, $Q_a = 0$.

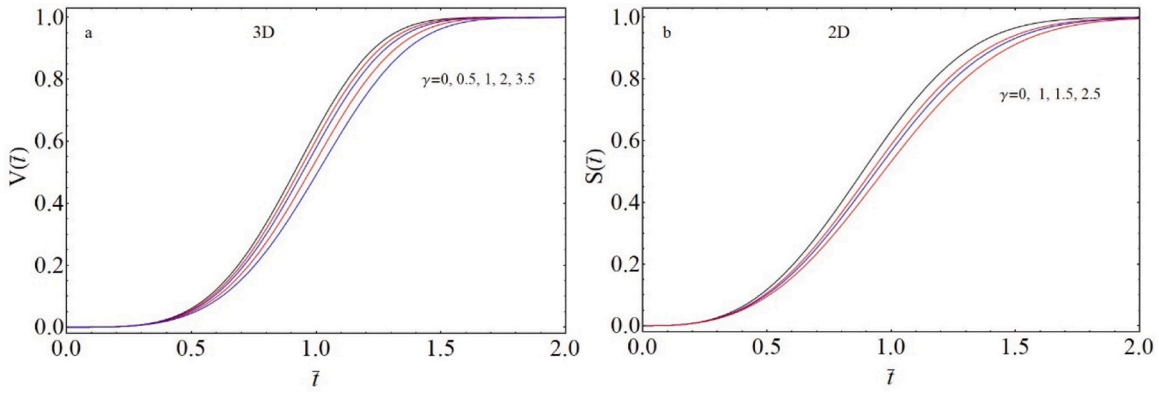

Fig. 8. Kinetics of phase transformations with correlated nucleation in 3D (panel *a*) and 2D (panel *b*). The kinetics for linear growth of spherical nuclei have been computed through Eq.3 using the nucleation rate of Fig. 5 (Section 2.3). In the curves, γ increases from top to bottom.

As explained in Section 2.1, once evaluated, the actual nucleation rate is used in Eq.3 to determine the volume fraction of the transformed phase. The outcome of the computation is reported in Fig. 8 for 3D (panel *a*) and 2D (panel *b*) transitions. In both panels an increase in the correlation strength, γ, causes a slight slow-down of the kinetics. In fact, the Avrami exponents of these kinetics are quite close to the values of the random case, $n = 4$ and $n = 3$ for 3D and 2D, respectively. For the curves of panel *a*) it is in the range $3.92 < n < 4$ and for panel *b*) in the interval $2.9 < n < 3$. Such behavior can be understood by considering the opposite role played by both nucleation and impingement between nuclei on the kinetics. On one hand, the higher the correlation degree the lower the number density of nuclei and the rate of transformation (Fig. 6). On the other hand, at higher correlation the overlaps between nuclei diminish, since nuclei are more isolated due to the greater excluded volume within which nucleation is prevented. Consequently, an unimpeded growth of nuclei increases the rate of transformation. The results of Fig. 8 indicate that the effect of the reduction in the density of nuclei is a little more important than that due to impingement. In fact, the small displacement of the Avrami exponent from the random case points to a nearly balancing of the two effects.

The weak dependence of $V(t)$ and $S(t)$ on γ entails that these are not the most appropriate experimental quantities to highlight correlation effects between nuclei in phase transitions. This conclusion has been previously reached in ref.[36] based on computer simulations. On the other hand, according to Figs.5,6 the impact of correlation on density of nucleation (and nucleation rate) is more important; this makes these quantities more suitable for experimental and computational studies on correlation effects in phase transformations [22]. Accordingly, in Appendix A we report a brief discussion on how spatial correlation effects could be validated by computer simulations.

3. Conclusions

In this work, we proposed a method for modeling the rate of formation of actual nuclei in phase transitions with spatially correlated nuclei and impingement between the growing nuclei. The case of hard-sphere interaction and linear growth has been studied. It is shown that the nucleation rate is the solution of an integral equation solved by successive iterations. To check the validity of the second order approximation, on which the method rests, the approach has been applied to KIMA compliant transformations, for which the exact solution is known. A very good agreement is obtained between KJMA solution and the second order expansion of the kinetics in terms of correlation functions.

The kinetics of nucleation has been studied as a function of the correlation radius, R_{hc}, in 2D and 3D. It is shown that the kinetics exhibits two regimes that are more distinct the larger the correlation degree. In the first, the kinetics is ruled by the correlated nucleation, like in the RSA process. In the second, the kinetics is ruled by the growth of the new phase and resemble the kinetics of the KJMA model.

The computation of the nucleation rate of the actual nuclei is required for determining the time evolution of the volume fraction of the new phase. This last quantity has been evaluated by solving a different stochastic approach than the one employed for Q_a, still using correlation functions at the same order of approximation. It is found that the rate of transformation decreases slightly with correlation radius. Such behavior has been ascribed to the reduction in the density of nuclei owing to correlation effects. In fact, the larger the correlation radius the larger the volume where nucleation is suppressed. Therefore, the fact that nuclei are more isolated in the nonrandom nucleation has a minor impact on the kinetics when compared to the reduction in nucleation rate.

CRediT authorship contribution statement

Massimo Tomellini: Writing – review & editing, Formal analysis, Data curation, Conceptualization.

Declaration of Competing Interest

The author declare that he has no known competing financial interests or personal relationships that could have appeared to influence the work reported in this paper.

Appendix A

A - Derivation of Eq.3

Eq.3 is derived by considering a set of different classes of dots. Dots belonging to different classes are distinguishable whereas dots belonging to the same class are indistinguishable. For two classes of dots the generalization of Eq.2 reads:

$$Q_0(\Delta_1,\Delta_2) = Q_0(\Delta_1)Q_0(\Delta_2)\exp\left[N_1N_2\int_{\Delta_1} d\boldsymbol{r}_1\int_{\Delta_2} d\boldsymbol{r}_2 g_2^{(1,2)}(\boldsymbol{r}_1,\boldsymbol{r}_2)\right] \tag{A1}$$

where N_1 and N_2 are the density of the two sets of dots and $Q_0(\Delta_i)$ $(i = 1,2)$ is given by Eq.2.

$Q_0(\Delta_1,\Delta_2)$ is the probability that no dots of class 1 and 2 lie in the domains Δ_1 and Δ_2, respectively. For m classes of dots with density N_i $(i = 1,2,..,m)$ we get

$$Q_0(\Delta_1,\Delta_2,\ldots,\Delta_m) = \exp\left[-\sum_{i=1}^{m} N_i|\Delta_i| + \frac{1}{2}\sum_{ij} N_iN_j\int_{\Delta_i} d\boldsymbol{r}_1\int_{\Delta_j} d\boldsymbol{r}_2 g_2^{(i,j)}(\boldsymbol{r}_1,\boldsymbol{r}_2)\right], \tag{A2}$$

where the 2-dots correlation function depends on the couple (i,j) and the factor ½ avoids double counting. The continuum limit of Eq. A2 is performed by labelling the classes with a continuous variable, say t'. The number of dots of the "t' -*class*" then becomes, $N_i \rightarrow \frac{dN(t')}{dt'}dt' = I_a(t')dt'$ with the integration domain $\Delta_{t',t}$, where t is the actual time and $0 < t' < t$. Eq.A2 eventually becomes

$$Q_0(\Delta_{0,t}) = \exp\left[-\int_0^t I_a(t')\left|\Delta_{t',t}\right|dt' + \int_0^t I_a(t')dt' \int_0^{t'} I_a(t'')dt'' \int_{\Delta_{t',t}} d\boldsymbol{r}_1 \int_{\Delta_{t'',t}} d\boldsymbol{r}_2 g_2(\boldsymbol{r}_1, \boldsymbol{r}_2, t', t'') \right]. \tag{A3}$$

Eq.A3 is the probability that no dots of the class t', whose number density is $I_a(t')dt'$, is located within the domain $\Delta_{t',t}$ (with $0 < t' < t$). In Eq.A3 each class is uniquely identified by t'. In modeling phase transformations, dots are nuclei centers, t' is the birth time of the nucleus and $t - t'$ the age of the nucleus. To determine the volume fraction of the new phase, at time t, $\Delta_{t',t}$ is set equal to the volume of the nuclei that start growing at time t'.

B- Expression of $F[Q_a]$

In terms of dimensionless units, the integral expression in Eq.9 is given by (see also section S3 in Supplementary Material),

$$F[Q_a] = -(D+1)X_{ex}\left(\int_0^1 Q_a(\tau_1) y^D(\tau_1) d\tau_1 \right)\left(1 + \frac{1}{2}(D+1)X_{ex} \int_0^1 Q_a(\tau_1) y^D(\tau_1) d\tau_1 \right) + \frac{(D(D+1))^2}{\Omega_D} X_{ex}^2 \times \int_0^1 Q_a(\tau_1) d\tau_1 \int_0^{\tau_1} Q_a(\tau_2) d\tau_2 \int_0^{\widetilde{\rho}(\tau_1)} x^{D-1} [H_1(\varphi_0(x) + \varphi_1(x, \tau_2)) + H_2 \varphi_2(x, \tau_1, \tau_2)] dx, \tag{B1}$$

where

$$y^D(\tau_1) = H(1-\rho_{hc})\left[H(\tau_1 + \rho_{hc} - 1)\rho_{hc}^D + H(1-\tau_1-\rho_{hc})(1-\tau_1)^D\right] + H(\rho_{hc}-1)\rho_{hc}^D \quad , \tag{B2}$$

$$\varphi_0(x) = \omega_D[\rho_{hc}, \rho_{hc};\, x], \tag{B3}$$

$$\varphi_1(x, \tau_2) = H(x - (\rho_{hc} - 1 + \tau_2))[H(1 - \tau_2 - \rho_{hc} - x)A(1-\tau_2, \rho_{hc}) + H(x - (1 - \tau_2 - \rho_{hc}))\omega_D[1-\tau_2, \rho_{hc};\, x]], \tag{B4}$$

and

$$\varphi_2(x, \tau_1, \tau_2) = [H(1 - x - \tau_1)A(1-\tau_2, \tau_1 - \tau_2) + H(x + \tau_1 - 1)\omega_D[1-\tau_2, \tau_1 - \tau_2;\, x]]. \tag{B5}$$

In the equations, $\rho_{hc} = \frac{R_{hc}}{at} = \frac{1}{\bar{t}}\left(\frac{\gamma}{3}\right)^{1/(D+1)}$ is the reduced radius of the correlation sphere where $\bar{t}$ is the reduced actual time and $\gamma = R_{hc}^{D+1}\frac{\pi I_0}{a}$. Eqs.B3,B4 refer to the case $\tau_1 - \tau_2 < \rho_{hc}$ (i.e. $R(t_1 - t_2) < R_{hc}$) and Eq.B5 to the case $\tau_1 - \tau_2 > \rho_{hc}$ (i.e. $R(t_1 - t_2) > R_{hc}$). Accordingly, in Eq.B1, $H_1 \equiv H(\rho_{hc} - (\tau_1 - \tau_2))$ and $H_2 \equiv 1 - H_1$. As regards the extreme of integration for x, namely $\widetilde{\rho}(\tau_1)$, and the integration domains for τ_1, and τ_2 in Eq.B1, we must refer to the three cases outlined in the text (see also Fig.3). To this end, the integration domains of the time variables are considered in Eq.B1 by multiplying the Q_a integrand for the Heaviside step functions reported below, together with the $\widetilde{\rho}(\tau_1)$ extreme of integration:

Case i) $1 - \rho_{hc} < \tau_2 < \tau_1$ i.e. $H(\tau_2 - (1 - \rho_{hc}))$ and $\widetilde{\rho}(\tau_1) = \rho_{hc}$

Case ii) $\tau_2 < 1 - \rho_{hc} < \tau_1$ i.e. $H((1 - \rho_{hc}) - \tau_2)H(\tau_1 - (1 - \rho_{hc}))$ and $\widetilde{\rho}(\tau_1) = \rho_{hc}$

Case iii) $\tau_2 < \tau_1 < 1 - \rho_{hc}$ i.e. $H((1 - \rho_{hc}) - \tau_1)$ and $\widetilde{\rho}(\tau_1) = 1 - \tau_1$

As stressed in the main text, for $\tau_1 - \tau_2 > \rho_{hc}$ (i.e. $R(t_1 - t_2) > R_{hc}$) only cases ii) and iii) hold.

In Eqs.B4,B5, $A(\rho_a, \rho_b) = \frac{\Omega_D}{D}\left[\rho_a^D - \rho_b^D\right]$ and $\omega_D[\rho_b, \rho_a;\, x]$ is the measure of $\Delta(\rho_b)\ \Delta(\rho_a)$, i.e. the volume of the sphere $\Delta(\rho_b)$ minus the overlap volume between $\Delta(\rho_a)$ and $\Delta(\rho_b)$. For $D = 2$ and $D = 3$ these volumes are given by:

$$\omega_2[\rho_b, \rho_a; x] = \rho_b^2\left[\pi - \cos^{-1}\frac{x^2 - (\rho_a^2 - \rho_b^2)}{2x\rho_b}\right] - \rho_a^2\cos^{-1}\frac{x^2 + (\rho_a^2 - \rho_b^2)}{2x\rho_a} + \frac{1}{2}\sqrt{4x^2\rho_b^2 - \left[x^2 - (\rho_a^2 - \rho_b^2)\right]^2}$$

and

$$\omega_3[\rho_b, \rho_a; x] = \pi\left[\frac{2}{3}(\rho_b^3 - \rho_a^3) - \frac{1}{12}x^3 + \frac{1}{2}x(\rho_a^2 + \rho_b^2) + \frac{(\rho_a^2 - \rho_b^2)^2}{4x}\right].$$

In these equations $\rho_k = \frac{R_k}{at}$ is the reduced radius.

Eq.9 in the main text was solved numerically by successive iteration, $Q_a^{(k)} = \exp(F[Q_a^{(k-1)}])$, starting from $Q_a^{(0)}(\bar{t}) = e^{-X_{ex}(\bar{t})} = e^{-\bar{t}^{(D+1)}}$ that is the KJMA solution. Fig.B1 shows the behavior of the relative integral error of the iterative process, η_k, as a function of the number of iterations, k: $\eta_k = 2\frac{\int[Q_a^{(k)} - Q_a^{(k-1)}]d\bar{t}}{\int[Q_a^{(k)} + Q_a^{(k-1)}]d\bar{t}}$. At $k = 9$ the error is lower than 10^{-4} and the two last kinetics (at $k = 9$ and $k = 8$) are practically indistinguishable in the entire time domain (not shown).

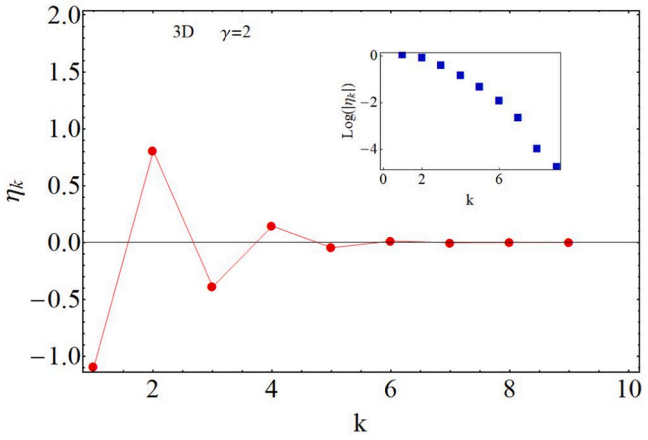

Fig.B1. Behavior of η_k *vs* k up to $k = 9$, for $D = 3$ and $\gamma = 2$ (solid circles). The solid line is a guide for the eyes. Inset: the decimal log of the absolute value of η_k is plotted as a function of k

C- Application of the model to computer simulations

The present approach, and its limitations mainly due to the truncation of the series in correlation functions, can be checked through computer simulations. The quantities introduced in the model are the rate of nucleation I_0, the linear growth rate of nuclei, a, and the correlation radius between pairs of nuclei, R_{hc}. The model shows that the kinetics of reduced number density, N, is a function of the single parameter γ, when reduced time, $\bar{t}$, is used. We recall that $N(\bar{t}) = \left(\frac{a}{I_0}\right)^{D/(D+1)} n_a(\bar{t})$, $\gamma = R_{hc}^{D+1}\frac{\pi I_0}{a}$ and $\bar{t} = \left(\frac{\Omega_D}{D(D+1)}\right)^{1/(D+1)} I_0^{1/(D+1)} a^{D/(D+1)} t$. Computer Simulations performed on a lattice and based on the assumptions of the present approach could be useful to validate the model. To this end, the quantities n_a and ξ should be extracted from the simulation and studied in the scaled form above reported. As anticipated in the main text, the number density of actual nuclei is the quantity that is more sensitive to the correlation, when compared to the transformed volume. We consider $N(\bar{t})$ and derive an analytical expression that can be useful for comparing the simulations to the results of the theory. We found that the $N(\bar{t})$ curves are in fair agreement with the following function:

$$N(\bar{t}) = (N_s - \alpha)\left(1 - e^{-\frac{\bar{t}}{N_s - \alpha}}\right) + \alpha\left(1 - e^{-\beta\bar{t}^2}\right), \tag{C1}$$

where $N_s = N(\infty)$ is the density at saturation and the parameters α and β are determined by fitting procedure. Fig.C1 displays the fit of Eq.C1 to the curves computed by the model for the 3D case. We found that Eq.C1 well describes also the N curves for the 2D case (not shown).

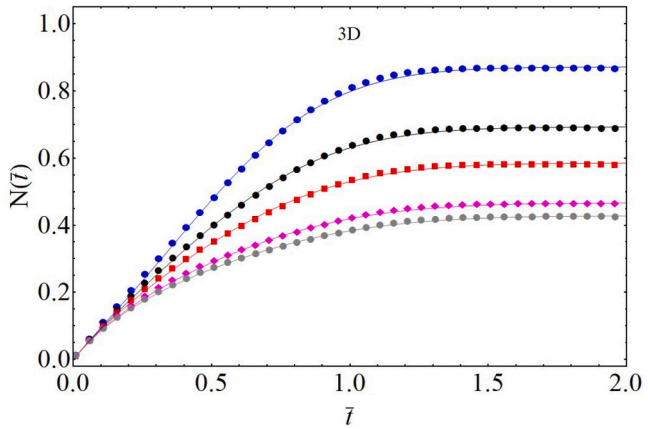

Fig.C1. Density of actual nuclei *vs* reduced time for various γ values. Solid symbols are the results of the theoretical approach (3D case). Solid lines are the best fits of Eq.C1 to the data for $\gamma = 0.05,\ 0.5,\ 1,\ 2,\ 2.5$. The γ value increases along the set of curves from top to bottom

The behavior of the parameters of Eq.C1 with γ are reported in Figs.C2 for 2D and 3D. The approach could be useful to get information on correlation when it is not possible to experimentally determine the pair distribution function. If the assumption of the model applies to the system and at a given time, t, the growth rate is determined together with the volume fraction and number density of actual nuclei, then an estimate of R_{hc} can be attempted. Considering ξ nearly independent of γ, (the volume fraction is not very

sensitive to γ), the experimental value of ξ provides $\bar{t}$ and, from t and a an estimate of I_0. This allows one to obtain the reduced density $N(\bar{t})$ that leads to an evaluation of γ through Eq.C1 and Fig.C2. Besides, from the definition of γ the correlation distance can be estimated.

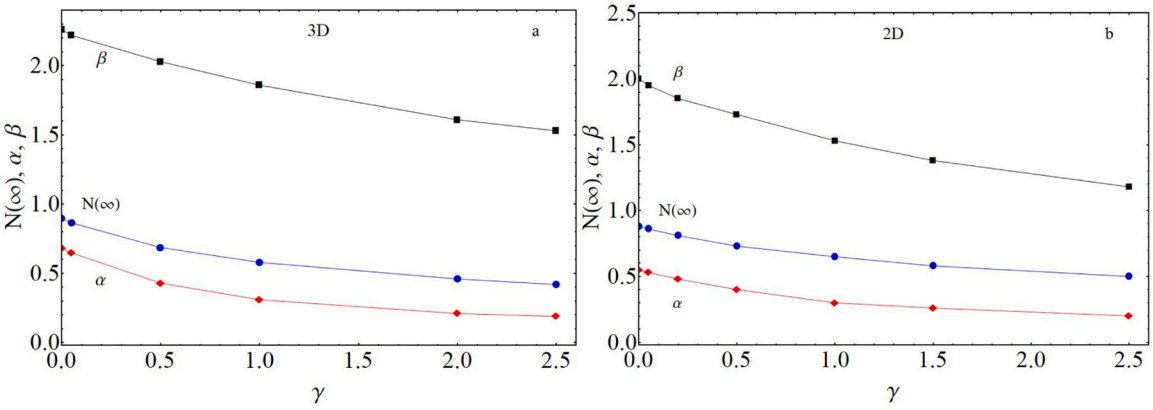

Fig.C2. Behavior of the parameters α, β, and $N(\infty)$ with γ for transformations in 3D (panel *a*) and 2D (panel *b*). Solid lines are a guide for the eyes

Appendix B. Supporting information

Supplementary data associated with this article can be found in the online version at doi:10.1016/j.physa.2025.130882.

Data Availability

Data will be made avaiable on request.

References

[1] (a) E. Clouet, Modeling of nucleation processes, in: D.U. Furrer, S.L. Semiatin (Eds.), ASM Handbook Vol. 22A, Fundamentals of Modeling for Metals Processing, ASM International, 2009, pp. 203–219;
(b) V. Dubrovskii, Fundamentals of nucleation theory. Nucleation Theory and Growth of Nanostructures. NanoScience and Technology, Springer, Berlin, Heidelberg, 2014, pp. 1–73.
[2] S. Karthika, T.K. Radhakrishnan, P. Kalaichelvi, A review of classical and nonclassical nucleation theories, Cryst. Growth Des. 16 (2016) 6663–6681.
[3] F.M. Kuni, A.K. Shchekin, A.P. Grinin, Theory of heterogeneous nucleation for vapor undergoing a gradual metastable state formation, Phys. Uspekhi 44 (4) (2001) 331–370.
[4] V. Raghavan, M. Cohen, Solid-state transformations, in: N.B. Hannay (Ed.), Changes of State, 5, Plenum Press, New York, 1975, pp. 67–127.
[5] R.D. Doherty, Diffusive phase transformations in the solid state, in: R.W. Chan, P. Haasen (Eds.), In: Physical Metallurgy, part II, Elsevier Science, 1996.
[6] J.W. Christian, The Theory of Transformation in Metals and Alloys, Pergamon, 1965.
[7] B. Rheingans, Y. Ma, F. Liu, E.J. Mittemeijer, Crystallisation kineticsof $Fe_{40}Ni_{40}B_{20}$ amorphous alloy, J. Non Cryst. Solids 362 (2013) 222–230.
[8] A.N. Kolmogorov, On the statistical theory of the crystallization of metals, URSS Bull. Acad. Sci. (Cl. Sci. Math. Nat.) 3 (1937) 355–359.
[9] W.A. Johnson, R.F. Mehl, Reaction kinetics in processes of nucleation and growth, Trans. AIME 135 (1939) 416–458.
[10] M. Avrami Kinetics of phase change I, J. Chem. Phys. 7 (1939) 1103-1112; ibid. II, 8 (1940) 212-224, ibid. III, 91941 177 184.
[11] J.S. Blazquez, F.J. Romero, C.F. Conde, A. Conde, A review of different models derived from classical Kolmogorov, Johnson and Mehl and Avrami (KJMA) theory to recover physical meaning in Solid-State transformations, Phys. Status Solidi (b) 259 (2022) 2100524.
[12] P. Bruna, D. Crespo, R. Gonzàlez-Cinca, On the validity of Avrami formalism in primary christallization, J. Appl. Phys. 100 (2006) 054907.
[13] R.A. Ramos, P.A. Rikvold, M.A. Novotny, Test of the Kolmogorov-Johnson-Mehl-Avrami picture of metastable decay in a model with microscopic dynamics, Phys. Rev. B 59 (1999) 9053–9069.
[14] J. Farjas, P. Roura, Microstructure development during isothermal crystallization, Phys. Rev. B 75 (2007) 184112.
[15] A.V. Teran, A. Bill, R.B. Bergmann, Time evolution of grain size distribution in random nucleation and growth crystallization process, Phys. Rev. B 81 (2010) 075319.
[16] B. Rheingans, E.J. Mittemeijer, Phase transformation kinetics: advanced modeling strategies, JOM 65 (9) (2013) 1145–1154.
[17] K. Shirzad, C. Viney, A critical review on application of the Avrami equations beyond materials science, J. R. Soc. Interface 20 (2023) 20230242.
[18] M. Fanfoni, M. Tomellini, The Johnson-Mehl-Avrami-Kolmogorov model: a brief review, Il Nuovo Cim. 20 (D) (1998) 1171–1182.
[19] M.J. Starink, Analysis of aluminum based alloys by calorimetry: quantitative analysis of reactions and reactions kinetics, Intern. Mater. Rev. 49 (3-4) (2004) 191–226.
[20] M. Tomellini, M. Fanfoni, Why phantom nuclei must be considered in the Johnson-Mehl-Avrami-Kolmogoroff kinetics, Phys. Rev. B 55 (1997) 14071–14073.
[21] A.E. Kuchma, A.K. Shchekin, Multicomponent condensation on the nucleation stage, J. Chem. Phys. 150 (5) (2019) 054104.
[22] A. Radisic, P.M. Vereecken, J.B. Hannon, P.C. Searson, F.M. Ross, Quantifying electrochemical nucleation and growth of nanoscale clusters using real-time kinetic data, Nano Lett. 6 (2) (2006) 238–242.
[23] G.E. Moehl, P.N. Bartlett, A.L. Hector, Using GISAXS to detect correlations between the locations of gold particles electrodeposited from an aqueous solution, Langmuir 36 (2020) 4432–4438.
[24] V. Tsakova, A. Milchev, Spatial distribution of electrochemically deposited clusters: a simulation study, J. Electroanal. Chem. 451 (1998) 211–218.
[25] M.E. Hyde, R.M.J. Jacobs, R.C. Compton, An electrodeposition study of the nucleation and growth of silver on boron doped diamond electrodes, J. Electroanal. Chem. 562 (2004) 61–72.

[26] Y. Sun, G. Zangari, Observation of Weibull, Lognormal, and Gamma distributions in electrodeposited Cu and Cu-Ag particles, Materials 16 (2023) 6452.
[27] L. Guo, P.C. Searson, Simulations of island growth and island spatial distribution during electrodeposition, Electrochem. SolidState Lett. 10 (2007) D76–D78.
[28] M. Tomellini, Spatial distribution of nuclei in progressive nucleation, Physica A Stat. Mech. Appl 496 (2018) 481–494.
[29] A.P. Grinin, F.M. Kuni, Y.S. Djikaev, Statistico-probabilistic approach to taking account of the vapor depletion in the kinetics of homogeneous nucleation: a free-molecular regime of droplet growth, J. Chem. Phys. 120 (4) (2004) 1846–1854.
[30] A.E. Kuchma, A.K. Shchekin, D.S. Martyukova, Nucleation stage of multicomponent bubbles of gases dissolved in a decompressed liquid, J. Chem. Phys. 148 (2018) 234103.
[31] S.D. Janssens, D. Vazquez-Cortes, E. Fried, Formation and morphology of closed and porous films grown from grains seeded on substrates: Two-dimensional simulations, Acta Mater. 225 (2022) 117555.
[32] M. Tomellini, R. Polini, Impact of seed density on continuous ultrathin nanodiamond film formation, Diam. Relat. Mater. 133 (2023) 109700.
[33] M. Tomellini, M. Fanfoni, M. Volpe, Spatially correlated nuclei: how the Johnson-Mehl-Avrami-Kolmogorov formula is modified in the case of simultaneous nucleation, Phys. Rev. B 62 (2000) 11300–11303.
[34] W.S. Tong, J.M. Rickman, K. Barmak, Impact of short-range repulsive interactions between nuclei on the evolution of a phase transformation, J. Chem. Phys. 114 (2001) 915–922.
[35] E. Pineda, T. Pradell, D. Crespo, Non-random nucleation and the Avrami kinetics, Philos. Mag. A Phys. Condens. Matter Struct. Defects Mech. Prop. 82 (2002) 107–121.
[36] P.R. Rios, J.C.P.T. Oliveira, V.T. Oliveira, J.A. Castro, Microstructural descriptors and cellular automata simulation of the effects of Non-random nuclei location on recrystallization in two dimensions, Mater. Res. 9 (2) (2006) 165–170.
[37] J.M. Rickman, K. Barmak, Kinetics of first order phase transitions with correlated nuclei, Phys. Rev. E 95 (2017) 022121.
[38] M. Tomellini, M. Fanfoni, M. Volpe, Phase transition kinetics in the case of nonrandom nucleation, Phys. Rev. B 65 (2002) 140301.
[39] M. Tomellini, M. Fanfoni, Connection between phantom and spatial correlation in the Kolmogorov– Johnson–Mehl–Avrami-model: a brief review, Phys. A 590 (2022) 126748.
[40] M.P. Shepilov, Kinetics of transformation for model with a diffusion law of growth of new-phase particles nucleated on active centers, Glass Phys. Chem. 30 (4) (2004) 291–299.
[41] M. Tomellini, M. Fanfoni, Eliminating overgrowth effects in Kolmogorov–Johnson–Mehl–Avrami model through the correlation among actual nuclei, Phys. A 333 (2004) 65–70.
[42] N.V. Alekseechkin, Extension of the Kolmogorov–Johnson–Mehl–Avrami theory to growth laws of diffusion type, J. Non Cryst. Solids 357 (2011) 3159–3167.
[43] (a) M. Fanfoni, M. Tomellini, Beyond the constraint underlying the Kolmogorov-Johnson-Mehl-Avrami model: inclusion of the spatial correlation, Eur. Phys. J. B. 34 (2003) 331–341;
(b) M. Tomellini, M. Fanfoni, Comparative study of approaches based on the differential critical region and correlation functions in modeling phase transformation kinetics, Phys. Rev. E. 90 (2014) 052406.
[44] M.J. Rost, L. Jacobse, M.T.M. Koper, Non-random island nucleation in the electrochemical roughening on Pt(111), Angew. Chem. Int. Ed. 62 (2023) e202216376.
[45] M.J. Rost, Nucleation and growth of nano-islands during surface reactions or alloying with increased lattice constant, J. Electrochem. Soc 170 (2023) 012504.
[46] V. Trofimov, Exclusion zone model of islands spatial distribution in molecular beam epitaxy, Thin Solid Films 380 (2000) 64–66.
[47] P. Schaaf, J. Talbot, Kinetics of random sequential adsorption, Phys. Rev. Lett. 62 (2) (1989) 175–178.
[48] Y. Qian, S. Li, Optimal three-dimensional particle shapes for maximally dense saturated packing, J. Chem. Phys. 161 (2024) 014505.
[49] S. Torquato, O.U. Uche, F.H. Stillinger, Random sequential addition of hard spheres in high Euclidean dimensions, Phys. Rev. E 74 (2006) 061308.